



1 **Chemical characteristics of PM_{2.5}: Impact of biomass burning at an**
2 **agricultural site of the North China Plain during a season of transition**

3 Linlin Liang¹, Guenter Engling^{2,3}, Chang Liu¹, Wanyun Xu¹, Xuyan Liu⁴, Yuan Cheng⁵, Zhenyu
4 Du⁶, Gen Zhang¹, Junying Sun¹, Xiaoye Zhang¹

5 ¹ State Key Laboratory of Severe Weather & Key Laboratory for Atmospheric Chemistry, Chinese
6 Academy of Meteorological Sciences, Beijing 100081, China

7 ² Division of Atmospheric Sciences, Desert Research Institute, Reno, NV 89512, USA

8 ³ Now at: California Air Resources Board, El Monte, CA 91731, USA

9 ⁴ National Satellite Meteorological Center, Beijing 100081, China

10 ⁵ School of Environment, Harbin Institute of Technology, Harbin 150001, China

11 ⁶ National Research Center for Environmental Analysis and Measurement, Beijing 100029 China

12 **Abstract:**

13 Biomass burning (BB) activities are ubiquitous in China, especially in North China, where
14 there is an enormous rural population and winter heating custom. In order to better understand
15 their impacts on aerosol chemical characteristics in rural and agricultural areas of the North China
16 Plain, BB tracers (i.e., levoglucosan (LG), mannosan (MN) and potassium (K⁺)), as well as other
17 chemical components were quantified at a rural site (Gucheng, GC) from 15 October to 30
18 November, during a transition heating season, when the field burning of agricultural residues was
19 becoming intense. The measured daily average PM_{2.5} concentrations of LG, MN and K⁺ during
20 this study were $0.79 \pm 0.75 \mu\text{g m}^{-3}$, $0.03 \pm 0.03 \mu\text{g m}^{-3}$ and $1.52 \pm 0.62 \mu\text{g m}^{-3}$. Due to the
21 planetary boundary layer development, carbonaceous components and BB tracers showed higher
22 levels at nighttime than daytime, while OM and secondary inorganic ions were enhanced during
23 daytime, likely due to enhanced photochemical activity. An episode with high levels of BB tracers
24 was encountered at the end of October, 2016, with high LG at $4.37 \mu\text{g m}^{-3}$. Based on the
25 comparison of chemical components during different BB periods, it appeared that biomass
26 combustion can obviously elevate carbonaceous components levels, whereas there seems to be
27 essentially no effect on secondary inorganic ions in the ambient air. Moreover, the LG/MN ratios
28 in different BB periods were consistent, while the LG/K⁺ ratio during intensive BB periods was



29 significantly elevated at times, with K^+ not increasing as much as LG during intensive BB
30 episodes. This indicated that there were other sources of K^+ in the study region, such as fireworks,
31 fertilizer use, or soil resuspension, which don't have variable contributions of K^+ during the
32 intensive BB periods; however, local soft wood and vegetation combustion can't be excluded,
33 which have efficient formation of levoglucosan during flaming fires.

34 **Keywords:** Biomass burning; Organic tracers; Levoglucosan; Mannosan; Potassium

35 1. Introduction

36 Particulate air pollution is attracting more and more concerns in China because of their
37 obvious adverse impact on visibility reduction, as well as health implication and regional or global
38 climate change (Kanakidou et al., 2009; Pope and Dockery, 2006; Chen et al., 2017).
39 Carbonaceous species, i.e., organic carbon (OC) and elemental carbon (EC), and water-soluble
40 inorganic ions, e.g., SO_4^{2-} , NO_3^- and NH_4^+ are the major components of ambient aerosols (Liang
41 et al., 2017; Du et al., 2014; Zheng et al., 2015; Tan et al., 2016). Biomass burning emissions
42 constitute a large source of ambient particulate pollution, especially for carbonaceous components,
43 i.e., primary organic carbon (POC) and black carbon (BC) on global scale (Bond et al., 2004; Tang
44 et al., 2018; Salma et al., 2017; Titos et al., 2017). As an important aerosol component, black
45 carbon from industrial and combustion emissions contributes to the enhanced $PM_{2.5}$ mass
46 concentrations and influences regional radiative forcing (Chen et al., 2017). Fresh biomass
47 burning aerosol was found to be mainly comprised of carbonaceous species which typically
48 constitutes 50-60% of the total particle mass (Hallquist et al., 2009). Yao et al. (2016) identified
49 approximately half of carbonaceous aerosols being contributed by biomass burning at Yucheng, a
50 rural site in the North China Plain.

51 Biomass burning emissions also represent a potentially large source of secondary organic
52 aerosol (SOA). The precursors and formation pathways of SOA from biomass burning emissions
53 were investigated by abundant field observations (e.g., Zhu et al., 2015; 2016; 2017; Adler et al.,
54 2011). Based on morphological particle analysis, Yao et al. (2016) investigated the smoke emitted
55 from biomass burning impacting SOA production. Sun et al. (2010) found that phenolic
56 compounds, which were emitted in large amounts from wood combustion, can form SOA at high



57 yields in aqueous-phase reactions. In addition, smoke from biomass burning can be transported
58 thousands of kilometers downwind from the source areas. Biomass burning aerosol from
59 Southeast Asia can be transported to China, Singapore and even further to North America (Liang
60 et al., 2017; Hertwig et al., 2015; Peltier et al., 2008). Based on molecular tracer measurements,
61 synoptic data as well as air mass back trajectory analysis, a fire episode was captured at a
62 background site of East China with smoke advected from Southeast Asia (Liang et al., 2017).

63 The North China Plain (NCP) is one of the most polluted regions in China. Severe haze–fog
64 of longer duration and more extensive coverage has occurred frequently in the NCP area,
65 especially during the seasons of autumn and winter. NCP covers one quarter of China's cultivated
66 land and yields 35% of the agricultural products in China (Boreddy et al., 2017). The rural
67 population in NCP is also large and dense, and biomass burning activities are common in this
68 region in form of cooking and heating. Intense fire activity typically occurs in October after the
69 corn harvest. Abundant smoke is emitted from agricultural burning, i.e., residential biofuel
70 combustion, open field burns, etc. Various field observations have investigated different aspects of
71 biomass burning, e.g., seasonal variations, chemical and physical properties of smoke particles,
72 spatial distribution, sources, transport, etc., in the NCP region (Cheng et al., 2013; Shen et al.,
73 2018; Sun et al., 2013; 2016; Boreddy et al., 2017; Yan et al., 2015). However, these field
74 investigations of the contribution of biomass burning to ambient aerosols in the NCP region were
75 concentrated on the city of Beijing (Cheng et al., 2013; Zheng et al., 2015; Duan et al., 2004).
76 Little field research about biomass burning was reported for rural areas in the NCP. In fact,
77 biomass burning activities are common in the rural areas of the NCP region, and the resulting
78 smoke aerosol can be transported to urban areas, e.g., the city of Beijing, resulting in haze
79 episodic events. Meanwhile, biomass burning studies at rural sites can provide valuable source
80 information of the biomass burning pollution in the North China region.

81 The objective of this study is to gain insights about the abundance of biomass burning smoke
82 during the autumn-winter transition season, following the corn harvest. In this paper, we focus on
83 quantifying multiple biomass burning tracers, i.e., LG, MN and K^+ as well as other chemical
84 species in $PM_{2.5}$ in GC during the autumn-winter transition biomass burning season. The study
85 results demonstrate the biomass burning pollution status in the rural atmosphere of North China



86 and explore the impact of biomass burning activities on the chemical properties of ambient
87 aerosols.

88 **2. Site description and experimental Methods**

89 **2.1 Site description**

90 Samples were collected at a rural site, Gucheng (GC, 39°09'N, 115°44'E; 15.2 m a.s.l),
91 located on a platform at the China Meteorological Administration farm in the town of Gucheng
92 (GC site), approximately 110 km southwest of Beijing and 35 km north of the city of Baoding
93 (population of about 5 million) in Hebei province, as shown in *Fig. S1*. The station is surrounded
94 by agricultural fields, with major crop species being corn and wheat. The dominant wind direction
95 at GC is southwest and northeast during the study period. This site is upwind of Beijing, when the
96 wind blows from the south or southwest, where heavily polluted cities and regions of Hebei
97 province, i.e., Baoding, Shijiazhuang, Xingtai, Handan, are located. Thus, it is an appropriate
98 station for representing the air pollution situation in the NCP region (Sheng et al., 2018; Chi et al.,
99 2018; Xu et al., 2019; Kuang et al., 2020).

100 Daytime and nighttime PM_{2.5} samples were collected from 15 October, 2016 to 23 November,
101 2016, by using PM_{2.5} High-volume (Hi-Vol) samplers (GUV-15HBL1, Thermo Fisher Scientific
102 CO., LTD), at the nominal flow rate of 1.13 m³ min⁻¹. All PM_{2.5} samples were collected on quartz
103 fiber filters, prebaked at 850 °C for at least 5 h to remove organic material. A total of 33 couples of
104 daytime/nighttime samples and 6 whole-day samples as well as 4 field blank samples were
105 collected during the sampling period. The filters were stored at -20 °C after sample collection.

106 **2.2 Experimental Methods**

107 **2.2.1 Anhydrosugar and water-soluble inorganic ion analysis**

108 The quartz filter samples were analyzed for biomass burning anhydrosugar tracers, i.e., LG
109 and MN, using an improved high-performance anion-exchange chromatography (HPAEC) method
110 with pulsed amperometric detection (PAD) on a Dionex ICS-5000+ system. LG and MN were
111 separated by a Dionex Carbopac MA1 analytical column and guard column with an aqueous
112 sodium hydroxide (NaOH, 480 mM) eluent at a flow rate of 0.4 mL min⁻¹. The detection limit of
113 LG and MN was 0.002 mg L⁻¹ and 0.005 mg L⁻¹, respectively. More details about the



114 HPAEC-PAD method can be found elsewhere (Iinuma et al., 2009).

115 The quartz filter samples were also analyzed for water-soluble inorganic ions by a Dionex
116 ICS-5000+ ion chromatograph, including three anions (i.e., SO_4^{2-} , NO_3^- , Cl^-) and five cations
117 (i.e., NH_4^+ , Ca^{2+} , Na^+ , K^+ and Mg^{2+}). The cations were separated on an Ionpac CS12 analytical
118 column and CG12 guard column with a 20 mM methanesulfonic acid as eluent at a flow rate of
119 1.0 mL min^{-1} , while the anions were separated on an Ionpac AS11-HC column and AG11-HC
120 guard column with 21.5 mM KOH eluent at a flow rate of 1.0 mL min^{-1} . The water-soluble
121 inorganic ion data were corrected by field blanks.

122 **2.2.2 Organic carbon/elemental carbon analysis**

123 OC and EC were measured on a punch (0.526 cm^2) of each quartz sample by a
124 thermal/optical carbon analyzer (DRI Model 2001, Desert Research Institute, USA), using the
125 Interagency Monitoring of Protected Visual Environments (IMPROVE) thermal evolution
126 protocol with reflectance charring correction. The analytical error of OC was within 10%, and one
127 sample of every 10 samples was selected at random for duplicate analysis. The detection limit of
128 OC was $0.82 \mu\text{g cm}^{-2}$ (Liang et al., 2017).

129 **2.2.3 Gas online monitoring (i.e., NO, NO₂, SO₂, O₃, CO and NH₃)**

130 During this campaign, commercial instruments from Thermo Fisher Scientific Co., LTD were
131 used to measure O_3 (TE 49C), $\text{NO}/\text{NO}_2/\text{NO}_x$ (Model 42CTL), CO (TE 48CTL), and SO_2
132 (TE43CTL), while NH_3 was measured by an ammonia analyzer (DLT-100, Los Gatos Research,
133 USA) at GC station. All measurement data quality was controlled according to standards described
134 elsewhere (Xu et al., 2019; Lin et al., 2011; Meng et al., 2018; Ge et al., 2018).

135 **2.2.4 Meteorological parameters**

136 The meteorological parameters, including air temperature, relative humidity (RH) and wind
137 speed on a 24-h resolution at the GC site are presented in Fig. 1. The wind speed was usually
138 lower than 1 m s^{-1} at the GC site, indicating that calm wind was most frequent, and unfavorable
139 dispersion conditions prevailed during the autumn-winter transition season. During the sampling
140 time from 15 October, 2016 to 23 November, 2016, the mean RH at GC was observed at 77%,
141 exhibiting moist conditions. These meteorological parameters indicate that GC was characterized
142 by humid and stagnant air masses.



143 2.2.5 Back trajectory and fire spot analysis

144 To characterize the transport pathways of the aerosol at the Gucheng site, back-trajectories
145 were calculated with the NOAA Hybrid Single-Particle Lagrangian Integrated Trajectory
146 (HYSPPLIT) model via NOAA ARL READY Website (<http://ready.arl.noaa.gov/HYSPLIT.php>).

147 To investigate the influence of biomass burning activities in surrounding areas, fire hot spot
148 counts were obtained from the Fire Information for Resource Management System (FIRMS)
149 (available at <https://firms.modaps.eosdis.nasa.gov/download/>).

150 3. Summary and implications

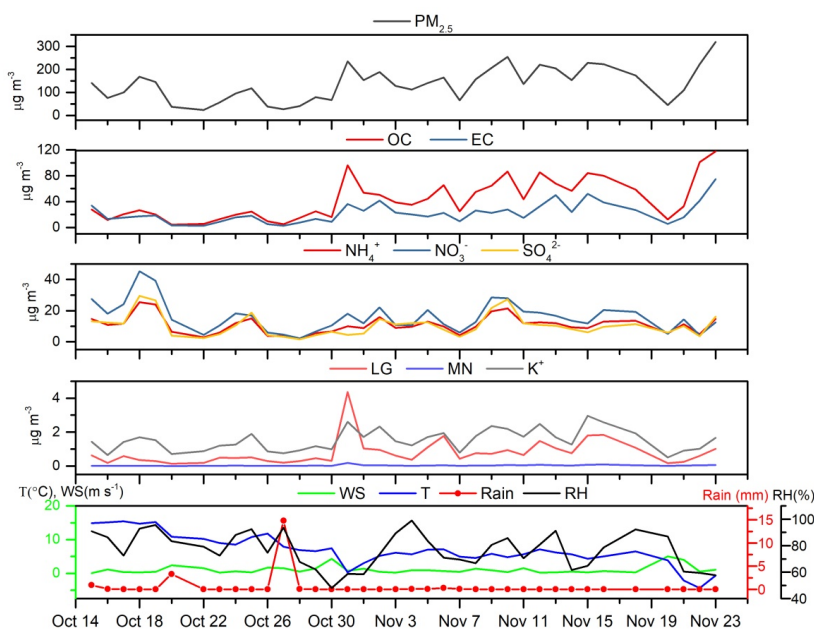
151 3.1 Characteristics of chemical components in PM_{2.5}

152 Fig. 1 describes the time-series variation obtained for daily PM_{2.5}, and its major
153 components (OC, EC, SO₄²⁻, NO₃⁻ and NH₄⁺), biomass burning tracers (LG, MN and K⁺) and
154 meteorological factors (temperature, RH, wind speed and rainfall) during the sampling period. The
155 mean concentrations and standard deviation of PM_{2.5}, the quantified components and
156 meteorological parameters for the whole study period are listed in Table 1. In this study, the mass
157 concentration of PM_{2.5} was reconstituted by the sum of carbonaceous components (1.6×OC + EC)
158 and inorganic ions (SO₄²⁻ + NH₄⁺ + NO₃⁻ + Cl⁻ + Ca²⁺ + Na⁺ + K⁺ + Mg²⁺). The average daily
159 PM_{2.5} mass concentration in the autumn-winter transition season at GC reached 137 ± 72.4 μg m⁻³,
160 ranging from 23.3 μg m⁻³ to 319 μg m⁻³, which is higher than during the severe winter haze in
161 January, 2013 at an urban site in Beijing (121.0 μg m⁻³) (Zheng et al., 2015). The mass
162 concentrations of these chemical species during the day are distributed as follows (from highest to
163 lowest): OC > EC > NO₃⁻ > SO₄²⁻ > NH₄⁺ > Cl⁻ > Ca²⁺ > K⁺ > Na⁺ > Mg²⁺. Organic matter (OM)
164 was the most abundant component, the daily average value of which was 70.4 ± 49.6 μg m⁻³,
165 accounting for nearly half (46.7%) of PM_{2.5} mass, indicating obvious organic pollution at the rural
166 site in the North China Plain during the sampling season.

167 Secondary inorganic aerosol (sulfate, SO₄²⁻; nitrate, NO₃⁻ and ammonium, NH₄⁺, SNA)
168 species, were the major water soluble ions, accounting for 82.8% of total water soluble ions, the
169 daily average values of which were 10.5 ± 6.87 μg m⁻³, 15.9 ± 9.29 μg m⁻³ and 10.9 ± 5.51 μg m⁻³
170 (Table 1). SNA species exhibited a synchronous temporal trend, while the NO₃⁻ concentrations



171 exceeded those of SO_4^{2-} at the GC site, in contrast to the results of previous studies, e.g., Tan et al.
172 (2016), who found SO_4^{2-} to be the dominant species in $\text{PM}_{2.5}$ during winter time in 2006 in Beijing.
173 SO_4^{2-} has previously been reported for many sites to be the dominant component of SNA in $\text{PM}_{2.5}$,
174 followed by NO_3^- and NH_4^+ (Duan et al., 2003; Yang et al., 2011; He et al., 2012). These findings
175 can likely be explained by the variation in SO_2 and NO_x emissions over the last decade in China
176 (Sun et al., 2016a; 2016b). SO_2 emissions have decreased as a result of desulfurization, whereas
177 NO_x emissions have increased as a result of industrialization and an increase in the number of
178 vehicles. Similarly, Chi et al., (2018) also found NO_3^- concentrations exceeded those of SO_4^{2-} at
179 both Beijing and GC sites during the winter time in 2016, although they observed that NH_4^+ was
180 the dominant component of SNA (the concentrations of SO_4^{2-} , NO_3^- and NH_4^+ were $14.0 \mu\text{g m}^{-3}$,
181 $14.2 \mu\text{g m}^{-3}$, and $24.2 \mu\text{g m}^{-3}$, respectively).



182
183 Fig. 1. Time-series variation obtained for $\text{PM}_{2.5}$ and its major components (OC , EC , SO_4^{2-} , NO_3^- and NH_4^+),
184 biomass burning tracers (LG , MN and K^+) and meteorological factors (temperature, RH , wind speed and rainfall)
185 at the GC site during the sampling period from 15 Oct to 23 Nov 2016.

186 The measured daily average concentrations of biomass burning tracers, i.e., LG , MN and K^+ in
187 $\text{PM}_{2.5}$ during our study were $0.79 \pm 0.75 \mu\text{g m}^{-3}$, $0.03 \pm 0.03 \mu\text{g m}^{-3}$ and $1.52 \pm 0.62 \mu\text{g m}^{-3}$ (Table
188 1). The anhydrosugar levels (LG and MN) in this study were both higher than those observed in



189 the city of Beijing during summer and winter seasons (Cheng et al., 2013; Yan et al., 2015). The
 190 highest concentrations of LG in Gucheng were observed on 31 October, 2016 with $4.37 \mu\text{g m}^{-3}$,
 191 which is a sharp increase (over 30 times) of the minimum concentration ($0.14 \mu\text{g m}^{-3}$) during that
 192 period. Accordingly, the $\text{PM}_{2.5}$ concentration during that period was also elevated (as high as 236
 193 $\mu\text{g m}^{-3}$) (Fig. 1).

194 Table 1. Average concentrations and the range of chemical components in $\text{PM}_{2.5}$ ($\mu\text{g m}^{-3}$) and meteorological
 195 data observed at GC site from 15/10/2016 to 23/11/2016.

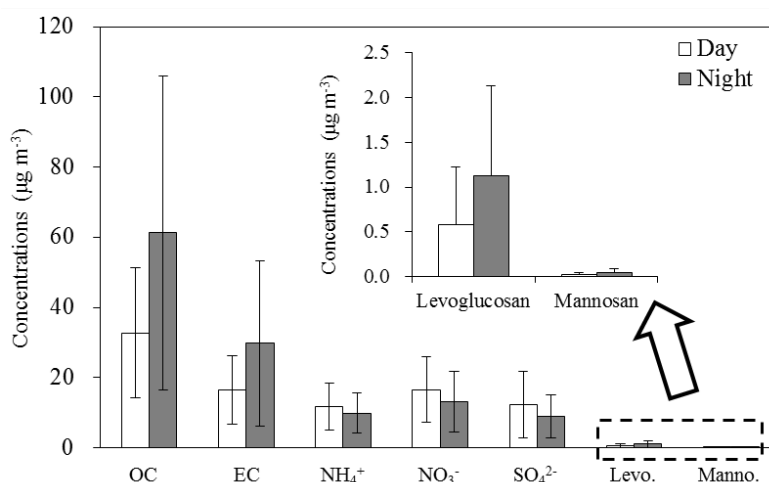
Species	Daytime (N = 34)		Nighttime (N = 33)		Whole period (N = 37)	
	Concentration	Range	Concentration	Range	Concentration	Range
$\text{PM}_{2.5}$ mass	117 ± 58.8	19.0 - 225	170 ± 116	21.1 - 465	137 ± 72.4	23.3 - 319
OC	26.8 ± 15.7	3.78 - 64.8	61.6 ± 49.5	2.88 - 175	44.0 ± 31.0	4.13 - 117
EC	13.4 ± 8.49	1.44 - 34.0	30.9 ± 28.5	2.21 - 129	21.7 ± 15.8	2.46 - 74.9
TC	49.3 ± 27.6	5.76 - 124	92.5 ± 73.6	5.10 - 289	65.8 ± 44.1	7.36 - 192
OC/EC	2.02 ± 1.26	1.09 - 3.31	2.25 ± 1.04	1.04 - 6.72	1.95 ± 0.60	0.83 - 3.10
SO_4^{2-}	12.1 ± 9.31	1.65 - 39.7	9.02 ± 6.22	1.55 - 23.2	10.5 ± 6.87	1.66 - 29.5
NO_3^-	16.9 ± 9.96	1.85 - 41.2	13.1 ± 8.52	1.56 - 38.0	15.9 ± 9.29	2.40 - 45.2
Cl^-	4.33 ± 2.30	0.82 - 9.46	6.08 ± 4.00	0.62 - 16.0	4.90 ± 2.46	0.93 - 9.37
NH_4^+	11.7 ± 6.76	1.84 - 26.0	10.0 ± 5.75	1.33 - 22.2	10.9 ± 5.51	1.99 - 25.4
K^+	1.43 ± 0.54	0.20 - 2.64	1.78 ± 0.95	0.22 - 4.19	1.52 ± 0.62	0.50 - 2.96
Mg^{2+}	0.26 ± 0.14	0.07-0.64	0.19 ± 0.09	0.06 - 0.38	0.14 ± 0.12	0.04 - 0.43
Ca^{2+}	2.24 ± 1.01	1.02-4.75	1.56 ± 0.08	0.77 - 3.56	1.54 ± 0.90	0.49 - 3.84
Na^+	0.44 ± 0.17	0.10 - 0.79	0.43 ± 0.24	0.10 - 1.31	0.42 ± 0.17	0.11 - 0.88
$\text{NO}_3^- / \text{SO}_4^{2-}$	1.67 ± 0.82	0.75 - 5.52	1.54 ± 0.57	0.74 - 3.50	1.65 ± 0.62	0.78 ± 3.96
Levogluconan	0.57 ± 0.62	0.05 - 3.74	1.10 ± 0.99	0.05 - 4.82	0.79 ± 0.75	0.14 - 4.37
Mannosan	0.024 ± 0.023	0.00 - 0.14	0.05 ± 0.04	0.00 - 0.21	0.03 ± 0.03	0.00 - 0.18
NO (ppb)	23.0 ± 14.7	2.07 - 56.0	45.9 ± 29.5	1.59 - 96.9	31.8 ± 18.3	1.81 - 68.5
NO_2 (ppb)	25.8 ± 10.4	8.18 - 51.6	29.3 ± 9.37	8.81 - 51.1	26.6 ± 8.74	8.62 - 51.4
SO_2 (ppb)	9.78 ± 4.96	3.11 - 22.5	9.63 ± 5.67	2.91 - 28.7	8.61 ± 4.04	3.37 - 20.4
CO (ppm)	0.96 ± 0.73	0.03 - 2.49	1.29 ± 1.04	0.02 - 3.26	1.05 ± 0.76	0.12 - 2.48
O_3 (ppb)	13.0 ± 9.10	1.42 - 41.84	5.00 ± 5.73	1.60 - 24.30	9.25 ± 5.78	1.67 - 24.0
NH_3 (ppb)	16.4 ± 11.3	1.68 - 46.2	18.3 ± 10.7	1.03 - 42.7	17.1 ± 9.88	1.46 - 44.4
Temperature (°C)	7.71 ± 4.01	-2.07-15.9	3.30 ± 4.69	-6.60 - 14.5	6.95 ± 4.58	-4.33 - 15.4
Relative Humidity (%)	68 ± 17	31 - 98	85 ± 14	34 - 100	77 ± 13	48 - 99
Wind speed (m s^{-1})	1.43 ± 1.17	0.09 - 5.65	0.79 ± 1.55	0.03 - 7.19	1.07 ± 1.14	0.04 - 5.02

196 During this campaign, the daily average RH value was observed at $77 \pm 13\%$, with a range
 197 from 48% to 99%, while the daily average wind speed averaged at $1.07 \pm 1.14 \text{ m s}^{-1}$, exhibiting
 198 moist and stable synoptic conditions at this rural site. Under low wind speeds and high RH,
 199 aerosol particles are very conducive to accumulate in the atmosphere. Moreover, there was rare
 200 precipitation during the sampling period at the GC site, except for two days, i.e., 20 and 27



201 October, 2016. High wind speed and precipitation can interrupt stable synoptic meteorological
202 conditions, enhancing the dilution and dispersion of pollutants in the air, and ultimately increased
203 wind speed and rainfall will cause opposite PM_{2.5} patterns (Fig. 1).

204 3.2 Day-night variations in the characteristics of PM_{2.5} chemical components

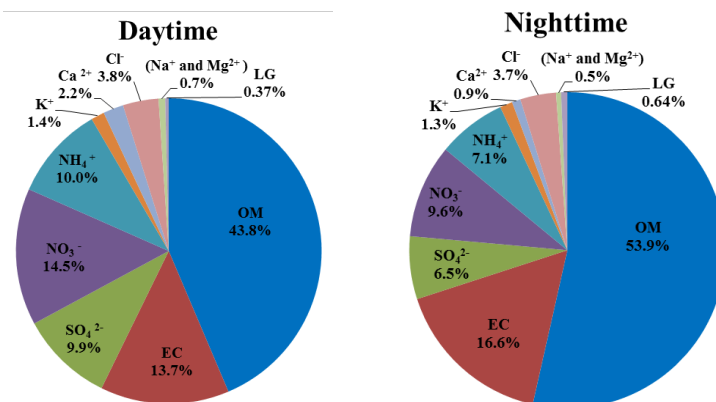


205
206 Fig. 2. Day and night distributions of mean concentrations of main chemical components in PM_{2.5} observed at GC
207 site during the sampling period.

208 The corresponding average mass concentrations and percent contributions of individual
209 chemical components to total estimated PM_{2.5} mass in daytime and nighttime during this
210 campaign are reported in Fig. 2 and Fig. 3. Time-series variations of PM_{2.5} and individual
211 components in daytime and nighttime during the sampling period are shown in *Fig. S2*. Generally,
212 carbonaceous components and biomass burning tracers exhibited higher levels during nighttime
213 than daytime, while secondary inorganic ions showed the opposite pattern, i.e., higher
214 concentrations during daytime than nighttime. In addition, the gap of carbonaceous components
215 and anhydrosugars between daytime and nighttime (two-fold) was more significant than for
216 secondary inorganic ions. That may be due to the variations of pollutant concentrations not only
217 being controlled by the chemical reactions but also being subject to the influence of the planetary
218 boundary layer (PBL) development. In the night, the PBL height decreases, compressing air
219 pollutants into a shallow layer, and subsequently resulting in faster accumulation and higher
220 concentrations of pollutants (Zheng et al., 2015; Zhong et al., 2018; 2019). Carbonaceous



221 components and anhydrosugars are not subject to significant differences in chemical reactions in
222 the ambient air between daytime and nighttime; thus, they will be mainly influenced by the
223 variations of the PBL height. Correspondingly, the contributions of OM and EC to $PM_{2.5}$ were
224 observed to be higher at nighttime (53.9% and 16.6%) than daytime (43.8% and 13.7%). The
225 contribution of LG to $PM_{2.5}$ during nighttime (0.64%) was also higher than that during daytime
226 (0.37%). However, unlike OM, secondary inorganic ions have an important formation path, i.e.,
227 photochemical processing, during daytime. Thus, the secondary species (SO_4^{2-} , NO_3^- and NH_4^+)
228 were enhanced during daytime due to photochemical formation (Fig. 2 and 3). Moreover, such an
229 enhancement in secondary transformations at daytime is more evident in terms of the mass
230 contributions of secondary inorganic ions to $PM_{2.5}$, that the contributions of SO_4^{2-} , NO_3^- and NH_4^+
231 to $PM_{2.5}$ decreased from daytime (9.9%, 14.5% and 10.0%) to nighttime (6.5%, 9.6% and 7.1%).



232
233 Fig. 3. Percent contributions of individual component mass concentrations to total estimated $PM_{2.5}$ mass in
234 daytime and nighttime during the sampling period.

235 In addition, the concentrations of other water-soluble inorganic ions, i.e., K^+ and Cl^- during
236 nighttime ($1.78 \pm 0.95 \mu g m^{-3}$ and $6.08 \pm 4.00 \mu g m^{-3}$) were higher than those in daytime ($1.43 \pm$
237 $0.54 \mu g m^{-3}$ and $4.33 \pm 2.30 \mu g m^{-3}$), while their contributions to $PM_{2.5}$ were reversed, due to the
238 significant accumulation and higher concentrations of pollutants during nighttime. The
239 contribution of the primary sources of Ca^{2+} , Mg^{2+} and Na^+ in nighttime were lower than those
240 during daytime, especially for Ca^{2+} , decreasing from 2.2% in daytime to 0.9% at nighttime (Fig. 3).
241 This may be because of these inorganic ions being emitted from primary sources, such as dust, soil
242 resuspension and sea salt, which are subject to more activity during the daytime and also
243 influenced by the airflow dynamics.



244 3.3 Biomass burning episodes and the impacts on chemical PM_{2.5} characteristics

245 Table 2. Concentrations of chemical components in PM_{2.5} aerosols and gaseous species collected at the GC site
 246 during the three biomass burning periods from 15 Oct to 23 Nov 2016.

Species	Period I (15-30 Oct)	Period II (31 Oct)		Period III (1 -23, Nov)	
	Minor biomass burning	Intensive biomass burning	Ratio*	Major biomass burning	Ratio*
	Concentration	Concentration		Concentration	Ratio*
PM _{2.5}	81.0 ± 44.5	235	2.91	172 ± 62.4	2.12
Levoglucosan	0.36 ± 0.14	4.37	12.1	0.92 ± 0.47	2.56
Mannosan	0.015 ± 0.005	0.18	12.0	0.042 ± 0.02	2.80
OC	16.2 ± 7.52	96.3	5.93	59.9 ± 25.3	3.69
EC	12.2 ± 5.85	36.0	2.96	29.1 ± 15.8	2.39
TC	28.4 ± 13.1	132	4.66	89.2 ± 38.8	3.14
SO ₄ ²⁻	10.3 ± 8.96	4.56	0.44	10.9 ± 5.55	1.06
NO ₃ ⁻	16.6 ± 12.9	18.1	1.09	15.2 ± 6.48	0.92
NH ₄ ⁺	10.1 ± 7.40	10.0	0.99	11.4 ± 4.19	1.13
K ⁺	1.16 ± 0.36	2.61	2.25	1.72 ± 0.62	1.48
Cl ⁻	3.46 ± 1.97	7.49	2.16	5.81 ± 2.33	1.68
OC/EC	1.53 ± 0.35	2.67	1.75	2.22 ± 0.53	1.45
NO ₃ ⁻ /SO ₄ ²⁻	1.74 ± 0.60	3.96	2.28	1.47 ± 0.39	0.84
LG/OC	0.025 ± 0.008	0.045	1.80	0.015 ± 0.006	0.60
LG/EC	0.039 ± 0.019	0.121	3.10	0.041 ± 0.027	1.05
LG/MN	24.9 ± 4.44	24.1	0.97	22.7 ± 6.71	0.91
LG/K ⁺	0.36 ± 0.081	1.67	4.64	0.52 ± 0.76	1.44
NO (ppb)	21.7 ± 12.5	21.7	1.00	39.5 ± 18.6	1.82
NO ₂ (ppb)	21.8 ± 4.95	26.5	1.22	30.0 ± 9.18	1.38
NO _x (ppb)	43.6 ± 16.3	48.2	1.11	69.5 ± 24.5	1.59
SO ₂ (ppb)	5.83 ± 2.46	8.04	1.38	10.6 ± 3.90	1.82
CO (ppm)	0.44 ± 0.33	0.70	1.59	1.51 ± 0.67	3.43
O ₃ (ppb)	9.79 ± 4.88	23.2	2.37	8.21 ± 5.47	0.84
NH ₃ (ppb)	14.3 ± 6.12	11.1	0.78	19.5 ± 10.8	1.36

247 *: indicates that the ratios of the intense BB period or major biomass burning period were divided by those from
 248 the minor BB period.

249 An episode with high biomass burning tracer levels was encountered on 31 October, 2016.
 250 The concentrations of levoglucosan in PM_{2.5} during this one-day episode (4.37 μg m⁻³) were
 251 significantly higher than those during typical transition season at the GC site (0.69 ± 0.47 μg m⁻³)
 252 (Fig.1). Here, we mainly distinguish three sub-periods based on daily LG concentrations during
 253 the time frame from 15 October to 23 November, 2016. The three periods were separated as
 254 follows: 15-30 October (Period I: Minor biomass burning), 31 October (Period II: Intensive
 255 biomass burning), 1- 23 November (Period III: Major biomass burning). Table 2 compares the
 256 concentrations of PM_{2.5} mass, chemical components and gases at the GC site during these three



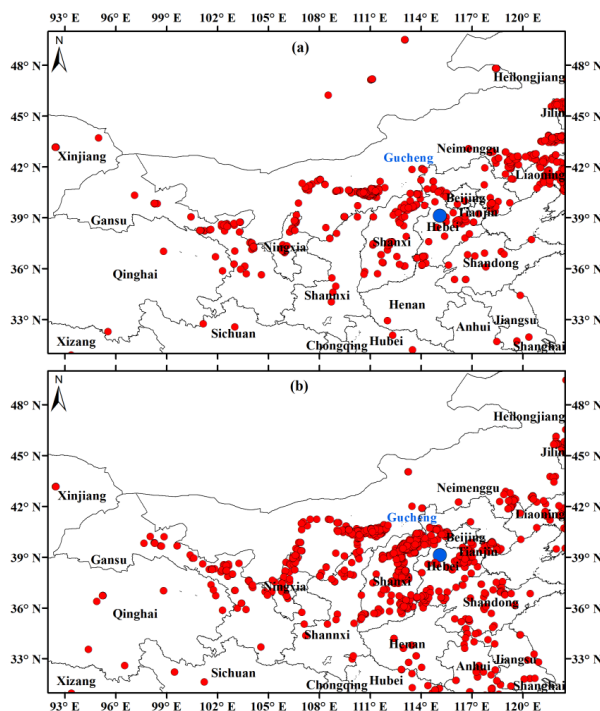
257 periods, as well as the ratios between the intensive and major BB periods to minor BB period.
258 Compared to typical autumn-winter transition time, the level of LG during the intensive BB
259 episode was about 12 times of that during the minor BB period. Furthermore, the concentrations
260 of OC and EC were also increased in the intensive and major BB periods (Table 2). For example,
261 during the intensive BB episode, OC was nearly 6 times of that during the minor BB period,
262 demonstrating that biomass burning influence can obviously contribute to carbonaceous aerosols
263 in the ambient rural environment. The episode on 31 October, 2016 with high PM_{2.5} levels was
264 apparently caused by intensive biomass combustion activities in the North China Plain.

265 During Period I, LG and MN were at low levels, with average concentrations of 0.36 ± 0.14
266 and $0.015 \pm 0.005 \mu\text{g m}^{-3}$. When entering into November, the heating season in the North China
267 region was commencing, resulting in the ambient levels of LG and MN increase to 0.92 ± 0.47
268 and $0.042 \pm 0.02 \mu\text{g m}^{-3}$ during period III, about 3 times of those in Periods I. Due to the frequent
269 heating activities in form of straw burning, we found the concentrations of PM_{2.5} mass,
270 carbonaceous components, K⁺ and Cl⁻ strongly increased during period III. Ambient
271 concentrations of OC and EC, for example, increased from $16.2 \pm 7.52 \mu\text{g m}^{-3}$ and $12.2 \pm 5.85 \mu\text{g}$
272 m^{-3} on average during the minor biomass burning period I to $59.9 \pm 25.3 \mu\text{g m}^{-3}$ and 29.1 ± 15.8
273 $\mu\text{g m}^{-3}$ in the major biomass burning period III.

274 However, compared to the carbonaceous components, the secondary inorganic aerosol
275 species (SO₄²⁻, NO₃⁻, NH₄⁺) exhibited a different pattern, i.e., showing no obvious differences
276 between BB period I and periods II and III. The ratios of SO₄²⁻, NO₃⁻, NH₄⁺ during periods II and
277 III to period I were all around 1.0 (Tab. 2), with no increasing trend. Moreover, the relationships
278 between LG and OC, EC during daytime and nighttime were both better than those with SNA (*Fig.*
279 *S3*). This pattern implied that biomass burning can evidently elevate the levels of carbonaceous
280 components but have no significant effect on secondary organic ions in the ambient air. This
281 finding is similar to the observations at Mt. Tai in China, where the concentrations of NH₄⁺ and
282 SO₄²⁻ were both higher in the minor BB period than those in the major BB period, while the
283 concentration pattern of NO₃⁻ was reversed, i.e., higher in the major BB period compared to the
284 minor BB period (Boreddy et al., 2017). However, the precursor gases of SNA, i.e., SO₂, NO, NO₂
285 and NH₃, were observed to have an increasing trend when biomass burning was prevalent during



286 periods II and III (the ratios of precursor gases of SNA during periods III to period I were in the
287 range of 1.38 to 1.82) (Table 2). The time-series variations of the gases (SO_2 , NO_x , NH_3 , CO and
288 O_3) and PBL during the sampling period are shown in *Fig. S4*. The primary emission gases were
289 exhibited negative relationships with PBL, while O_3 exhibited obvious positive relationship with
290 PBL. The average concentration of CO clearly increased from 0.44 ± 0.33 ppm in period I to 1.51
291 ± 0.67 ppm in period III, which illustrates that biomass burning was an important resource for CO
292 in the ambient air (Tab. 2), similar to the findings of Jung et al. (2014) observed at Daejeon, Korea,
293 during the rice harvest period.

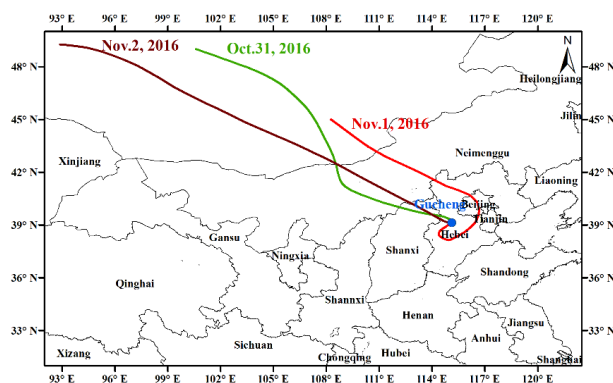


294
295 Fig.4. Fire spots at GC site and the surrounding provinces from (a) 15-30 October, 2016 and (b) 1-23, November,
296 2016, observed by MODIS Terra satellites (blue dot is GC station).

297 The combustion of biomass, especially of agricultural residues (e.g., wheat and corn straw)
298 is very common in the rural areas in North China during the autumn-winter transition period.
299 During the autumn harvest season in North China, wheat and corn straw burning is common
300 practice, resulting in more abundant fire spots observed during period III than period I (Fig. 4).
301 The intense biomass burning event on 31 October, 2016 was also supported by air mass back



302 trajectory analysis (Fig. 5), performed with the TrajStat software. Based on the 48 h back
303 trajectories at the GC site at 00:00 (UTC time) on 1 November, 2016, the air mass at the GC site
304 was restricted in the region of Beijing-Tianjing-Hebei, the polluted area where fire spots were
305 numerous. However, on the previous and following day of this episode, i.e., 31 October and 2
306 November, 2016 onward, the air masses arriving in GC were advected from Northwest Mongolia,
307 where mostly desert areas are present, with less farm land and rare biomass burning activities (Fig.
308 5).



309

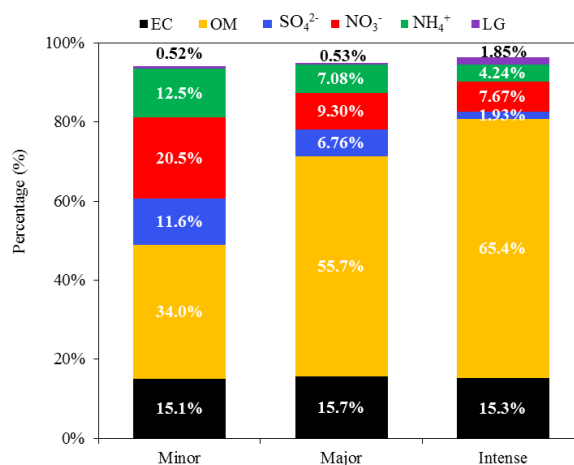
Fig. 5. 48 h back trajectories at 500 m at GC site from 31 October to 2 November, 2016.

310

311 Mean percentiles of major components in $PM_{2.5}$ with respect to different biomass burning
312 pollution periods at GC site during the sampling time are shown in Fig. 6. With the variation of
313 biomass burning pollution periods, the EC fraction seems to exhibit no obvious change and the
314 OC fraction increased significantly, while the contributions of sulfate, nitrate and ammonium to
315 $PM_{2.5}$ all decreased sharply (Fig. 6). This suggests that organic aerosol species become more
316 important for biomass burning pollution periods, concerning their contribution to the $PM_{2.5}$, while
317 EC has no such character. The OM percentage during intense biomass burning period II was
318 65.4%, about double of that during the minor biomass burning period (34.0%), indicating that
319 there was a large fraction of OM in $PM_{2.5}$ originating from biomass burning at the GC site during
320 intensive BB period II. Opposite to OM, contributions of secondary inorganic ions to $PM_{2.5}$
321 significantly decreased with the biomass burning pollution becoming more severe. The
322 contributions of SO_4^{2-} , NO_3^- and NH_4^+ to $PM_{2.5}$ during the minor BB episode (11.6%, 20.5% and
323 12.5%) obviously declined during the intense BB episode (1.73%, 7.73% and 4.24%). This

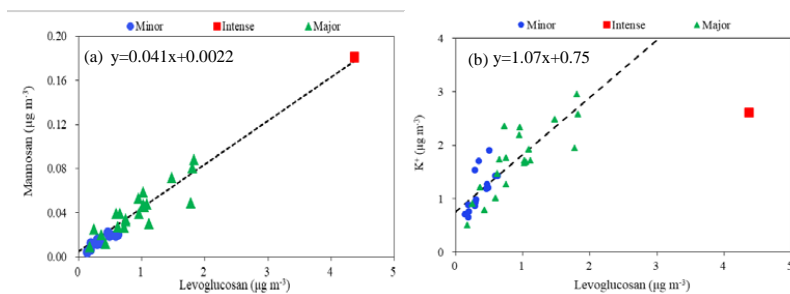


324 phenomenon further illustrates that biomass burning emissions can substantially increase the
325 ambient levels of organic aerosol, while not affecting the contributions of secondary inorganic
326 aerosols.



327
328 Fig. 6. Mean percentiles of major components in PM_{2.5} with respect to different biomass burning pollution periods
329 at GC site during the sampling time.

330 3.4 Relationships among tracers during different biomass burning pollution 331 periods



332
333 Fig. 7. Scatter plots of (a) levoglucosan versus mannosan, (b) levoglucosan versus K⁺

334 The LG/MN ratios during minor, major and intense biomass pollution periods were
335 observed at high values, i.e., 24.1, 24.1, 22.6, respectively (Tab. 2). However, the LG/K⁺ ratios
336 during the three periods (minor, major and intense biomass burning periods) varied considerably
337 (0.36, 0.52, 1.67) (Tab. 2). The scatter plots between LG and MN and K⁺ are shown in Fig. 7. The
338 relationship between LG and MN in the three periods followed one line, especially for period II



339 (red dot), which was located far from the concentrated plots of periods I and III, yet it was still on
340 the same regression line of the fitting curve (Fig. 7a). In contrast, the relationship between LG and
341 K^+ did not show a consistent pattern as that of LG versus MN, with the red dot of period II being
342 off from the fitted regression line (Fig. 7b). The LG/K^+ ratios during minor and major BB periods
343 (0.36 and 0.52) were similar to those during a biomass burning episode at an urban site of Beijing
344 during summer time ($Lev/K^+ = 0.51$), an urban site in Guangzhou (0.29) and an suburban site in
345 Zhuhai (0.4) during the dry season (Zhang et al., 2015). This LG/K^+ ratio during the intense BB
346 period II was observed at 1.67, which was significantly higher than that in periods I and III.

347 This high value of LG/K^+ ratio is probably the most representative of the local BB aerosol,
348 similar to the smoke aerosols from soft wood combustion (China fir and red pine) (Sang et al.,
349 2013; 2020). Similarly, the LG/K^+ ratios observed in Austria were also in the range of 0.91 to 1.7
350 during winter time, which were attributed mainly to wood burning in households (Caseiro et al.,
351 2009). Based on the results of biomass source combustion studies (Engling et al., 2009; Chantara
352 et al., 2019), comparing LG to K^+ , it appears that there is a large enrichment of LG in wood or
353 vegetation burning with efficient formation of LG during the flaming phase. There was a time of
354 strong process decrease in temperature at Gucheng site, the average daily temperature was sharply
355 decreased from 7.5°C at 30 Oct, 2016 to 0.31°C at 31 Oct, 2016 and the average temperature at the
356 night of 31 Oct, 2016 was even decreased to -3.4°C (Fig.1). Thus, it must be many combustion
357 taken places around the sampling site for heating, by burning straws, branches, as well as local
358 soft woods, since these fuels are also commonly used in rural areas of North China, i.e., pine,
359 poplar, China fir, etc. Moreover, the reason for this phenomenon maybe also due to other sources
360 of K^+ in the study region, such as fireworks, fertilizers, soil resuspension, etc. (Drewnick et al.,
361 2006; Urban et al., 2012; Cheng et al., 2013). During intensive biomass combustion periods, the
362 contributions from other sources of K^+ exhibit no or little variation, causing K^+ to not increase as
363 rapidly as LG, which is a unique source tracer from biomass burning in ambient aerosols.

364 4. Summary and implications

365 Biomass burning activities are ubiquitous in China, especially in North China, where
366 enormous rural populations are present, with a common winter heating custom. Anhydrosugars,
367 including levoglucosan and mannosan, and water-soluble potassium ion were employed as



368 molecular tracers to investigate the characteristics of biomass burning activities as well as their
369 impact on chemical properties of ambient aerosols in rural areas of North China. The measured
370 daily average concentrations of LG, MN and K^+ in $PM_{2.5}$ during a transition heating season, from
371 15 October to 30 November, 2016 were $0.79 \pm 0.75 \mu\text{g m}^{-3}$, $0.03 \pm 0.03 \mu\text{g m}^{-3}$ and $1.52 \pm 0.62 \mu\text{g}$
372 m^{-3} . The daily PBL development caused carbonaceous components and biomass burning tracers to
373 be higher at nighttime than daytime, while the patterns of secondary inorganic ions (SO_4^{2-} , NO_3^-
374 and NH_4^+) were opposite, which were enhanced during daytime due to photochemical formation.
375 Due to intense emissions and contribution of stable synoptic conditions, an episode with extreme
376 biomass burning tracer levels was encountered on 31 October, 2016, with concentrations of LG as
377 high as $4.37 \mu\text{g m}^{-3}$. Comparing the chemical composition between different biomass burning
378 periods, it was apparent that biomass burning can considerably elevate the levels of organic
379 components, while not showing a significant effect on the production of secondary inorganic ions,
380 although their precursors were observed at increased levels. In addition, it's interesting that the
381 LG/MN ratios in different biomass burning periods were similar, while the LG/ K^+ ratios during
382 the intensive BB period were abnormally higher than those in the minor and major periods. This
383 may be due to local soft wood combustion in the surrounding area, which have a more efficient
384 formation mechanism of levoglucosan than K^+ during flaming fires. On the other hand, this may
385 imply that there were other sources of K^+ in the study region, such as fireworks, fertilizers, soil
386 resuspension. Thus, based on the results from this study, governmental restrictions on biomass
387 burning emissions should be expanded, not only focusing on controlling open burning activities of
388 crop residues, but also including residential burning activities of biofuels, e.g., straws, woods or
389 other vegetations in the North China Plain, especially during the winter heating season.

390

391 **Data availability.** The data used in this study are available from the corresponding author
392 upon request (lianglinlin@cma.gov.cn).

393 **Author contributions.** LL designed conducted all observations and drafted the paper. GE
394 revised the paper and improved the English writing. XL drew the Fig.4 and 5. CL, WX, YC, ZD,
395 GZ, JS and XZ interpreted the data and discussed the results. All authors approved the final
396 version for publication.



397 **Competing interests.** The authors declare that they have no conflict of interest.

398 **Special issue statement.** This article is part of the special issue “In-depth study of air
399 pollution sources and processes within Beijing and its surrounding region (APHH-Beijing)
400 (ACP/AMT interjournal SI)”. It is not associated with a conference.

401 **Acknowledgements.** This research is supported by the Beijing Natural Science Foundation
402 (8192055) and CAMS Fundamental Research Funds (No. 2017Z011). The authors would like to
403 acknowledge Yingli Yu and Ye Kuang for their help with PM_{2.5} samples collection; Hongbing
404 Cheng for help with chemical analyses.

405 **Financial support.** This research has been supported by the Beijing Natural Science
406 Foundation (8192055), State Environmental Protection Key Laboratory of Sources and Control of
407 Air Pollution Complex (SCAPC201701) and CAMS Fundamental Research Funds (No.
408 2017Z011). Financial support was also provided partly by the Ministry of Science and
409 Technology (MOST) of Taiwan (MOST 103-2113-M-007-005).

410 **References:**

411 Boreddy, S. K. R., Kawamura, K., Okuzawa, K., Kanaya, Y., and Wang, Z.: Temporal and diurnal
412 variations of carbonaceous aerosols and major ions in biomass burning influenced aerosols
413 over Mt. Tai in the North China Plain during MTX2006, *Atmos. Environ.*, 154, 106-117,
414 <http://dx.doi.org/10.1016/j.atmosenv.2017.01.042>, 2017.

415 Caseiro, A., Bauer, H., Schmidl, C., Pio, C. A., and Puxbaum, H.: Wood burning impact on PM₁₀
416 in three Austrian regions, *Atmos. Environ.*, 43, 2186-2195,
417 <https://doi.org/10.1016/j.atmosenv.2009.01.012>, 2009.

418 Chantara, S., Thepnuan, D., Wiriya, W., Prawan, S., and Tsai, Y. I.: Emissions of pollutant gases,
419 fine particulate matters and their significant tracers from biomass burning in an open-system
420 combustion chamber, *Chemosphere*, 224, 407-416.
421 <https://doi.org/10.1016/j.chemosphere.2019.02.153>, 2019.

422 Chen, J., Li, C., Ristovski, Z., Milic, A., Gu, Y., Islam, M. S., Wang, S., Hao, J., Zhang, H., He, C.,
423 Guo, H., Fu, H., Miljevic, B., Morawska, L., Thai, P., Lam, Y. F., Pereira, G., Ding, A.,
424 Huang, X., and Dumka, U. C.: A review of biomass burning: Emissions and impacts on air
425 quality, health and climate in China, *Sci. Tot. Environ.*, 579, 1000-1034,
426 <https://doi.org/10.1016/j.scitotenv.2016.11.025>, 2017.

427 Cheng, Y., Engling, G., He, K. B., Duan, F. K., Ma, Y. L., Du, Z. Y., Liu, J. M., Zheng, M., and
428 Weber, R. J.: Biomass burning contribution to Beijing aerosol, *Atmos. Chem. Phys.*, 13,
429 7765–7781, <https://doi.org/10.5194/acp-13-7765-2013>, 2013.



- 430 Chi, X., He, P., Jiang, Z., Yu, X., Yue, F., Wang, L., Li, B., Kang, H., Liu, C., and Xie, Z.: Acidity
431 of aerosols during winter heavy haze events in Beijing and Gucheng, China, *J. Meteorol. Res.*,
432 32, 14-25, <https://doi.org/10.1007/s13351-018-7063-4>, 2018.
- 433 Drewnick, F., Hings, S. S., Curtius, J., Eerdekens, G., and Williams, J.: Measurement of fine
434 particulate and gas-phase species during the New Year's fireworks 2005 in Mainz, Germany,
435 *Atmos. Environ.*, 40, 4316-4327, <https://doi.org/10.1016/j.atmosenv.2006.03.040>, 2006.
- 436 Du, Z. Y., He, K. B., Cheng, Y., Duan, F. K., Ma, Y. L., Liu, J. M., Zhang, X. L., Zheng, M., and
437 Weber, R.: A yearlong study of water-soluble organic carbon in Beijing I: Sources and its
438 primary vs. secondary nature, *Atmos. Environ.*, 92, 514-521,
439 <https://doi.org/10.1016/j.atmosenv.2014.04.060>, 2014.
- 440 Duan, F. K., Liu, X. D., He, K. B., Lu, Y. C. and Wang, L.: Atmospheric aerosol concentration
441 level and chemical characteristics of water-soluble ionic species in wintertime in Beijing,
442 China, *J. Environ. Monit.*, 5, 569-573, <https://doi.org/10.1039/B303691J>, 2003.
- 443 Ge, B. Z., Wang, Z. F., Lin, W. L., Xu, X. B., Li, J., Ji, D. S., and Ma, Z.Q.: Air pollution over the
444 north china plain and its implication of regional transport: a new sight from the observed
445 evidences, *Environ. Pollut.*, 166, 29-38, <https://doi.org/10.1016/j.envpol.2017.10.084>, 2017.
- 446 Engling, G., Lee, J. J., Tsai, Y. W., Lung, S. C. C., Chou, C. C. K., and Chan, C. Y.: Size resolved
447 anhydrosugar composition in smoke aerosol from controlled field burning of rice straw,
448 *Aerosol Sci. Tech.*, 43, 662-672, <https://doi.org/10.1080/02786820902825113>, 2009.
- 449 He, K. B., Zhao, Q., Ma, Y. L., Duan, F. K., Yang, F. M., Shi, Z. B., and Chen, G.: Spatial and
450 seasonal variability of PM_{2.5} acidity at two Chinese megacities: insights into the formation
451 of secondary inorganic aerosols, *Atmos. Chem. Phys.*, 12, 1377-1395,
452 <https://doi.org/10.5194/acp-12-1377-2012>, 2012.
- 453 Hertwig, D., Burgin, L., Gan, C., Hort, M., Jones, A., Shaw, F., Witham, C., and Zhang, K.:
454 Development and demonstration of a Lagrangian dispersion modeling system for real-time
455 prediction of smoke haze pollution from biomass burning in Southeast Asia, *J. Geophys. Res.*:
456 *Atmos.*, 120, 12605-12630, <https://doi.org/10.1002/2015JD023422>, 2015.
- 457 Jung, J., Lee, S., Kim, H., Kim, D., Lee, H., and Oh, S.: Quantitative determination of the
458 biomass-burning contribution to atmospheric carbonaceous aerosols in Daejeon, Korea,
459 during the rice-harvest period, *Atmos. Environ.*, 89, 642-650,
460 <https://doi.org/10.1016/j.atmosenv.2014.03.010>, 2014.
- 461 Kanakidou, M., Seinfeld, J. H., Pandis, S. N., Barnes, I., Dentener, F. J., Facchini, M. C., Van
462 Dingenen, R., Ervens, B., Nenes, A., Nielsen, C. J., Swietlicki, E., Putaud, J. P., Balkanski, Y.,
463 Fuzzi, S., Horth, J., Moortgat, G. K., Winterhalter, R., Myhre, C. E. L., Tsigaridis, K., Vignati,
464 E., Stephanou, E. G., and Wilson, J.: Organic aerosol and global climate modelling: a review,
465 *Atmos. Chem. Phys.*, 5, 1053-1123, <https://doi.org/10.5194/acp-5-1053-2005>, 2005.
- 466 Kuang, Y., Xu, W. Y., Lin, W. L., Meng, Z. Y., Zhao, H. R., Ren, S. X. Zhang, G., Liang, L. L., and
467 Xu, X. B.: Explosive morning growth phenomena of NH₃ on the North China Plain: Causes
468 and potential impacts on aerosol formation, *Environ. Pollut.*,



- 469 <https://doi.org/10.1016/j.envpol.2019.113621>, in press, 2020.
- 470 Lin, W. L., Xu, X. B., Sun, J. Y., Liu, X. W., and Wang, Y.: Background concentrations of reactive
471 gases and the impacts of long-range transport at the jinsha regional atmospheric background
472 station, *Science China (Earth Sciences)*, 54, 1604-1613, 2011.
- 473 .Meng, Z. Y., Xu, X. B., Lin, W. L., Ge, B. Z., Xie, Y. L., Song, B., Jia, S. H., Zhang, R., Peng, W.,
474 Wang, Y., Cheng, H. B., Yang, W., and Zhao, H. R.: Role of ambient ammonia in particulate
475 ammonium formation at a rural site in the North China Plain, *Atmos. Chem. Phys.*, 18, 167–
476 184, <https://doi.org/10.5194/acp-18-167-2018>, 2018.
- 477 Peltier, R. E., Hecobian, A. H., Weber, R. J., Stohl, A., Atlas, E. L., Riemer, D. D., Blake, D. R.,
478 Apel, E., Campos, T., and Karl, T.: Investigating the sources and atmospheric processing of
479 fine particles from Asia and the Northwestern United States measured during INTEX B,
480 *Atmos. Chem. Phys.*, 8, 1835-1853, <https://doi.org/10.5194/acp-8-1835-2008>, 2008.
- 481 Pope, C. A., and Dockery, D. W.: Health effects of fine particulate air pollution: lines that connect,
482 *J. Air Waste Manage.*, 56, 709-742, <https://doi.org/10.1080/10473289.2006.10464485>, 2006.
- 483 Sang, X. F., Zhang, Z. S., Chan, C. Y., and Engling, G.: Source categories and contribution of
484 biomass smoke to organic aerosol over the southeastern Tibetan plateau, *Atmos. Environ.*, 78,
485 113-123, <https://doi.org/10.1016/j.atmosenv.2012.12.012>, 2013.
- 486 Sang, X. F., Fu, H. X., Zhang, Y. N., Ding, X., Wang, X. M., Zhou, Y. N., Zou, L. L., Zellmer, G.
487 F., and Engling, G.: Carbonaceous aerosol emitted from biofuel household stove combustion
488 in South China, *Atmosphere*, in proof., 2020.
- 489 Shen, X. J., Sun, J. Y., Zhang, X. Y., Zhang, Y. M., Wang, Y. Q., Tan, K. Y., Wang, P., Zhang, L.,
490 Qi, X. F., Che, H. Z., Zhang, Z., Zhong, J. T., Zhao, H. R., and Ren, S. X.: Comparison of
491 submicron particles at a rural and an urban site in the North China Plain during the December
492 2016 heavy pollution episodes, *J. Meteorol. Res.*, 32, 14-25,
493 <https://doi.org/10.1007/s13351-018-7060-7>, 2018.
- 494 Sun, K., Liu, X. G., Gu, J. W., Li, Y. P., Qu, Y., An, J. L., Wang, J. L., Zhang, Y. H., Hu, M., and
495 Zhang, F.: Chemical characterization of size-resolved aerosols in four seasons and hazy days
496 in the megacity Beijing of China, *J. Environ. Sci.*, 32, 155-167,
497 <https://doi.org/10.1016/j.jes.2014.12.020>, 2015.
- 498 Sun, Y. L., Zhang, Q., Anastasio, C., and Sun, J.: Insights into secondary organic aerosol formed
499 via aqueous-phase reactions of phenolic compounds based on high resolution mass
500 spectrometry, *Atmos. Chem. Phys.*, 10, 4809-4822, <https://doi.org/10.5194/acp-10-4809-2010>,
501 2010.
- 502 Sun, Y., Du, W., Fu, P., Wang, Q., Li, J., Ge, X., Zhang, Q., Zhu, C., Ren, L., Xu, W., Zhao, J., Han,
503 T., Worsnop, D. R., and Wang, Z.: Primary and secondary aerosols in Beijing in winter:
504 sources, variations and processes, *Atmos. Chem. Phys.*, 16, 8309-8329,
505 <https://doi.org/10.5194/acp-16-8309-2016>, 2016a.
- 506 Sun, Y. L., Jiang, Q., Xu, Y. S., Ma, Y., Zhang, Y. J., Liu, X. G., Li, W. J., Wang, F., Li, J., Wang, P.,
507 and Li, Z. Q.: Aerosol characterization over the North China Plain: Haze life cycle and



- 508 biomass burning impacts in summer, *J. Geophys. Res. Atmos.*, 121, 2508-2521,
509 <https://doi.org/10.1002/2015JD024261>, 2016b.
- 510 Sun, Y. L., Wang, Z. F., Fu, P. Q., Yang, T., Jiang, Q., Dong, H. B., Li, J., and Jia, J. J.: Aerosol
511 composition, sources and processes during wintertime in Beijing, China, *Atmos. Chem. Phys.*,
512 13, 4577-4592, <https://doi.org/10.5194/acp-13-4577-2013>, 2013.
- 513 Tan, J. H., Duan, J. C., Zhen, N. J., He, K. B., and Hao, J. M.: Chemical characteristics and source
514 of size-fractionated atmospheric particle in haze episode in Beijing, *Atmos. Res.*, 167, 24-33,
515 <https://doi.org/10.1016/j.atmosres.2015.06.015>, 2016.
- 516 Tang, R., Wu, Z., Li, X., Wang, Y., Shang, D., Xiao, Y., Li, M., Zeng, L., Wu, Z., Hallquist, M., Hu,
517 M., and Guo, S.: Primary and secondary organic aerosols in summer 2016 in Beijing, *Atmos.*
518 *Chem. Phys.*, 18, 4055-4068, <https://doi.org/10.5194/acp-18-4055-2018>, 2018.
- 519 Urban, R. C., Lima-Souza, M., Caetano-Silva, L., Queiroz, M. E. C., Nogueira, R. F. P., Allen, A.
520 G., Cardoso, A. A., Held, G., and Campos, M. L. A. M.: Use of levoglucosan, potassium, and
521 water-soluble organic carbon to characterize the origins of biomass-burning aerosols, *Atmos.*
522 *Environ.*, 61, 562-569, <https://doi.org/10.1016/j.atmosenv.2012.07.082>, 2012.
- 523 Wang, Z., Wang, T., Guo, J., Gao, R., Xue, L. K., Zhang, J. M., Zhou, Y., Zhou, X. H., Zhang, Q.
524 Z., Wang, W.X., 2012. Formation of secondary organic carbon and cloud impact on
525 carbonaceous aerosols at Mount Tai, North China, *Atmos. Environ.*, 46, 516-527,
526 <https://doi.org/10.1016/j.atmosenv.2011.08.019>, 2012.
- 527 Xu, W., Kuang, Y., Zhao, C., Tao, J., Zhao, G., Bian, Y., Yang, W., Yu, Y., Shen, C., Liang, L.,
528 Zhang, G., Lin, W., and Xu, X.: NH₃-promoted hydrolysis of NO₂ induces explosive growth
529 in HONO, *Atmos. Chem. Phys.*, 19, 10557-10570,
530 <https://doi.org/10.5194/acp-19-10557-2019>, 2019
- 531 Xu, X., Zhang, H., Lin, W., Wang, Y., Xu, W., and Jia, S.: First simultaneous measurements of
532 peroxyacetyl nitrate (PAN) and ozone at Nam Co in the central Tibetan Plateau: impacts from
533 the PBL evolution and transport processes, *Atmos. Chem. Phys.*, 18, 5199-5217,
534 <https://doi.org/10.5194/acp-18-5199-2018>, 2018.
- 535 Yan, C. Q., Zheng, M., Sullivan, A. P., Bosch, C., Desyaterik, Y., Andersson, A., Li, X. Y., Guo, X.
536 S., Zhou, T., Gustafsson, Ö., and Collett, J. L.: Chemical characteristics and light-absorbing
537 property of water-soluble organic carbon in Beijing: Biomass burning contributions, *Atmos.*
538 *Environ.*, 121, 4-12, <https://doi.org/10.1016/j.atmosenv.2015.05.005>, 2015.
- 539 Yang, F. M., Tan, J. H., Zhao, Q. Du, Z. Y., He, K. B., Ma, Y. L., Duan, F. K., Chen, G. and Zhao,
540 Q.: Characteristics of PM_{2.5} speciation in representative megacities and across China, *Atmos.*
541 *Chem. Phys.*, 11, 5207-5219, <https://doi.org/10.5194/acp-11-5207-2011>, 2011.
- 542 Yao, L., Yang, L. X., Chen, J. M., Wang, X. F., Xue, L. K., Li, W. J., Sui, X., Wen, L., Chi, J. W.,
543 Zhu, Y. H., Zhang, J. M., Xu, C. H., Zhu, T., and Wang, W. X.: Characteristics of
544 carbonaceous aerosols: Impact of biomass burning and secondary formation in summertime
545 in a rural area of the North China Plain, *Sci. Tot. Environ.*, 557-558,
546 <https://doi.org/10.1016/j.scitotenv.2016.03.111>, 2016.



- 547 Zhang, Z., Gao, J., Engling, G., Tao, J., Chai, F., Zhang, L., Zhang, R., Sang, X., Chan, C. Y., Lin,
548 Z., and Cao, J.: Characteristics and applications of size-segregated biomass burning tracers in
549 China's Pearl River Delta region, *Atmos. Environ.*, 102, 290-301,
550 <https://doi.org/10.1016/j.atmosenv.2014.12.009>, 2015.
- 551 Zheng, G. J., Duan, F. K., Su, H., Ma, Y. L., Cheng, Y., Zheng, B., Zhang, Q., Huang, T., Kimoto,
552 T., Chang, D., Pöschl, U., Cheng, Y. F., and He, K. B.: Exploring the severe winter haze in
553 Beijing: the impact of synoptic weather, regional transport and heterogeneous reactions,
554 *Atmos. Chem. Phys.*, 15, 2969-2983, <https://doi.org/10.5194/acp-15-2969-2015>, 2015.
- 555 Zheng, M., Salmon, L. G., Schauer, J. J., Zeng, L., Kiang, C. S., Zhang, Y., and Cass, G. R.:
556 Seasonal trends in PM_{2.5} source contributions in Beijing, China, *Atmos. Environ.*, 39,
557 3967-3976, <https://doi.org/10.1016/j.atmosenv.2005.03.036>, 2005.
- 558 Zhong, J. T., Zhang, X. Y., and Wang, Y. Q.: Reflections on the threshold for PM_{2.5} explosive
559 growth in the cumulative stage of winter heavy aerosol pollution episodes (HPEs) in Beijing,
560 *Tellus B*, 71, 1-7, <https://doi.org/10.1080/16000889.2018.1528134>, 2019.
- 561 Zhong, J. T., Zhang, X. Y., Wang, Y. Q., Liu, C., and Dong, Y. S.: Heavy aerosol pollution
562 episodes in winter Beijing enhanced by radiative cooling effects of aerosols, *Atmos. Res.*,
563 209, 59-64, <https://doi.org/10.1016/j.atmosres.2018.03.011>, 2018.
- 564 Zhu, C., Kawamura, K., and Kunwar, B.: Effect of biomass burning over the western North
565 Pacific Rim: wintertime maxima of anhydrosugars in ambient aerosols from Okinawa, *Atmos.*
566 *Chem. Phys.*, 15, 1959-1973, <https://doi.org/10.5194/acp-15-1959-2015>, 2015.
- 567 Zhu, C. S., Cao, J. J., Tsai, C. J., Zhang, Z. S., and Tao, J.: Biomass burning tracers in rural and
568 urban ultrafine particles in Xi'an, China, *Atmos. Pollut. Res.*, 8, 614-618,
569 <https://doi.org/10.1016/j.apr.2016.12.011>, 2017.
- 570 Zhu, Y. H., Yang, L. X., Kawamura, K., Chen, J. M., Ono, K., Wang, X. F., Xue, L. K., and Wang,
571 W. X.: Contributions and source identification of biogenic and anthropogenic hydrocarbons
572 to secondary organic aerosols at Mt. Tai in 2014, *Environ. Pollut.*, 220, 863-872,
573 <https://doi.org/10.1016/j.envpol.2016.10.070>, 2017.